Supplemental Information

Ionically Dispersed Fe(II)-N and Zn(II)-N in Porous Carbon for Acidic Oxygen Reduction Reaction

Sihui Liang,[a] Renjie Chen,[c] Peiwen Yu,[a] Mei Ni,[a] Qiao Zhang,[a,d] Xiaoling Zhang,[a*] Wen Yang[a,b*]

1 Experimental Section

1.1 Materials and Methods

Analytical grade 2-methylimidazole was purchased from Innochem Chemical Reagents, China. Iron (II) phthalocyanine was was provided by TCI. The commercial Pt/C catalyst is nominally 20% by wt carbon black, Zinc oxide and Nafion were acquired from Alfa. Dimethyl sulfoxide (DMSO) was purchased from Beijing Tongguang Fine Chemical Company, China. All of the chemicals used in this experiment were analytical grade and used without further purification.

1.2 Characterization

Structure and morphology of studied samples were characterized by X-ray diffraction (XRD, Bruker D8 Advance, 2.2 kw, Cu Kα radiation), transmission electron microscopy (TEM, JEOL JEM 2011, 200 kV), nitrogen adsorption-desorption at 77 K using the nonlocal density functional theory (NLDFT) and Barrett-Joyer-Halenda (BJH) methods, assuming a microporous/mesoporous model. The C K-edge, N K-edge of Near-edge X-ray absorption fine structure spectra (NEXAFS) were measured at 4B9B@Beijing Synchrotron Radiation Facility. The X-ray photoelectron spectroscopy (XPS) analysis was performed on an PHI QUANTERA-II using monochromatic Al Kα radiation (25 W, 15 kV). The metal content was determined by Inductively Coupled Plasma-Atomic Emission Spectroscopy (ICP-OES). The XAFS measurement for Fe K-edge (7710 eV) was acquired at the beamline 1W1B station of the Beijing Synchrotron Radiation Facility, China. The Fe K-edge XANES data were recorded in a fluorescence mode. Fe foil, Fe_2O_3, FePc were used as references. The storage ring was held at 2.5 GeV with an average electron current of 250 mA. The X-rays were monochromatized with Si(111) double-crystals. The acquired EXAFS data were extracted and processed according to standard procedures using the ATHENA module implemented in the IFEFFIT software package. The k^3-weighted EXAFS spectra were obtained by subtracting the post-edge background from the overall absorption and then normalizing with respect to the edge-jump step. ^{57}Fe Mössbauer spectra were measured at room

temperature using a Topologic 500A spectrometer and a proportional counter. A $^{57}Co(Rh)$ source, moving with a constant acceleration mode, was used as the γ-ray radioactive source. The velocity was calibrated by a standard α-iron foil.

1.3 Catalyst Synthesis

The preparation route of Fe-Zn/S/N/C-1000 is illustrated in Scheme 1. The precursor was pretreated by ball milling. Typically, 1.62 g ZnO, 3.28 g 2-methylimidazole (MeIM) and FePc were mixted, 200 μL DMSO was added as a sulfur source by pipette, and the mixture was ball milled for 30 min. The resulting mixture was kept at 50 °C for 24 h under vacuum, followed by pyrolysis in a tubular furnace at different temperatures (700, 800, 900, 1000 °C) under N_2 stream. After holding at the peak temperature for 1 h, the product was allowed to cool to room temperature. The optimal catalyst was prepared at a pyrolysis temperature of 1000 °C. Fe-Zn/N/C-1000 was synthesized using the same procedure, except for replacing DMSO by EtOH, and Zn/S/N/C-1000 was synthetisized by the same procedure and using DMSO, except that no FePc in was added.

1.4 Electrochemical Measurements

Voltammetry measurements were performed on a CHI 760D electrochemical workstation (Shanghai Chenhua, China) at room temperature, using a three-electrode configuration in 0.5 M H_2SO_4 or 0.1 M $HClO_4$ solution and a glassy carbon rotating ring disk electrode (RDE, 4 mm of disk outer diameter, Pine Research Instrumentation, USA), with the rotating rate varying from 400 to 2025 rpm. A platinum foil and Ag/AgCl (saturated KCl) were used as counter and reference electrodes, respectively. Five mg of the catalyst was dispersed in 350 μL ethanol and 95 μL 5 wt% Nafion, then mixed ultrasonically for 30 min to form a well dispersed black ink. Eight μL of the suspension was pipetted on a glassy carbon electrode, whose surface was precleaned and dried under infrared illumination.

The solutions were saturated with high-purity O_2 or N_2 at least 30 min before each experiment, and the flow of O_2 or N_2 was maintained during the measurement. The negative-direction sweep of potential was from 1.2 V to 0 V (RHE) at a rate of 5 mV s^{-1} with an electrode rotation speed of 1600 rpm.

Koutecky–Levich plots (j^{-1} vs. $\omega^{-1/2}$) were analysed in 0.5 M H_2SO_4 with varying rotation speed. The electron transfer number (n) was calculated using the Koutecky–Levich equation:

$$j^{-1} = j_k^{-1} + j_L = j_k^{-1} + (0.62nFCD^{2/3}\gamma^{-1/6}\omega^{1/2})^{-1}$$

where j indicates the measured current density, j_k and j_L are the kinetic- and diffusion limited current densities, respectively, ω indicates the angular velocity ($\omega = 2\pi N$, where N is the rotation rate), n is the electron transfer number, F is the Faraday constant (F = 96485 C mol^{-1}), C is the bulk concentration of O_2 ($C = 1.2*10^{-3}$ mol L^{-1}), D is the diffusion coefficient of O_2 in the electrolyte ($D = 1.9*10^{-5}$ cm^2 s^{-1}), γ is the kinetic viscosity of the electrolyte (γ = 0.01 cm^2 s^{-1}).

Turnover frequencies (TOFs) of the catalysts were calculated according to the following equation[1]:

$$TOF\left[e\ site^{-1}\ s^{-1}\right] = \frac{J_K \times M_{Fe}}{(Catalyst\ Loading) \times c_{Fe} \times c_{D,Fe} \times F}$$

where j_k, M_{Fe}, c_{Fe}, $c_{D,Fe}$, and F indicate the mass-transfer-corrected kinetic current density, the atomic weight of Fe (55.845 g_{Fe} mol^{-1}), Fe concentration in the catalyst, relative absorption area for doublets obtained by Mössbauer spectroscopy, and the Faraday constant (96,485 C mol^{-1}). We assumed that D1 is the active site for the ORR in acidic media. The Fe concentrations for Fe-Zn/N/C-1000 and Fe-Zn/S/N/C-1000 were 0.7 wt.% and 1.2 wt.%, respectively.

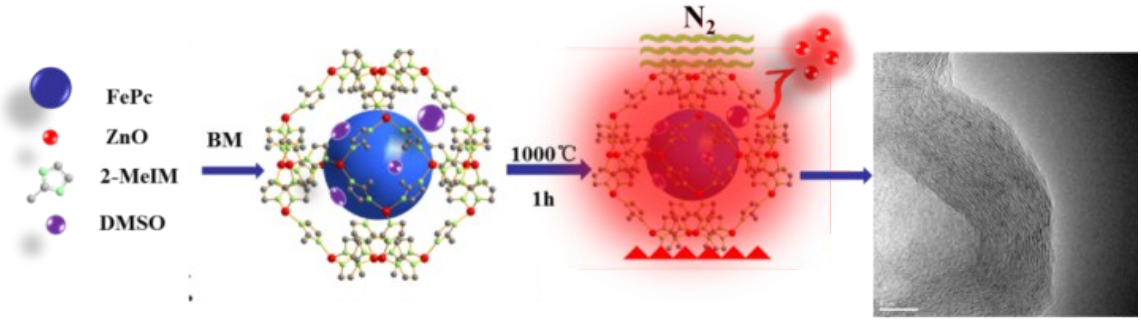

Fig S1. Illustration of the fabrication process of Fe-Zn/S/N/C-1000.

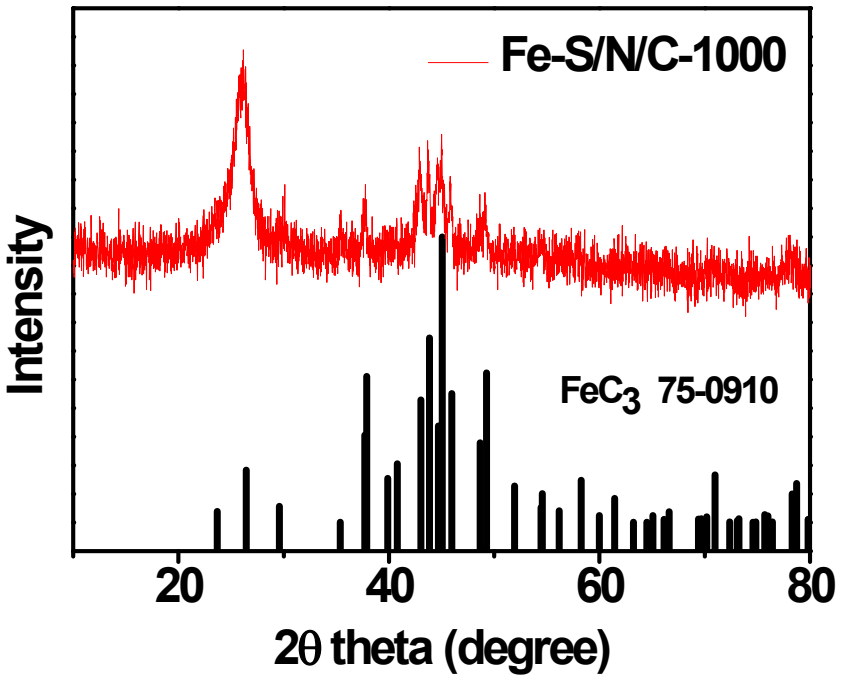

Fig S2. XRD patterns of the resulting catalysts of Fe-S/N/C-1000.

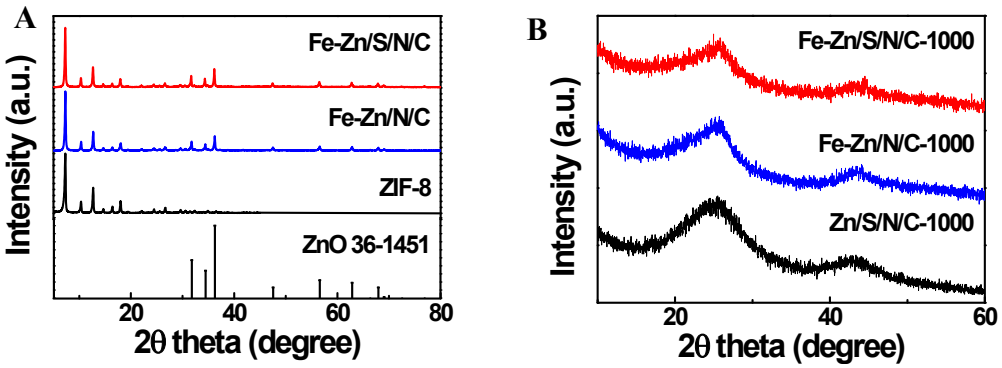

Fig S3. A) XRD patterns of ZnO, ZIF-8, Fe-Zn/N/C, Fe-Zn/S/N/C before prolysis. B) XRD patterns of the resulting catalysts.

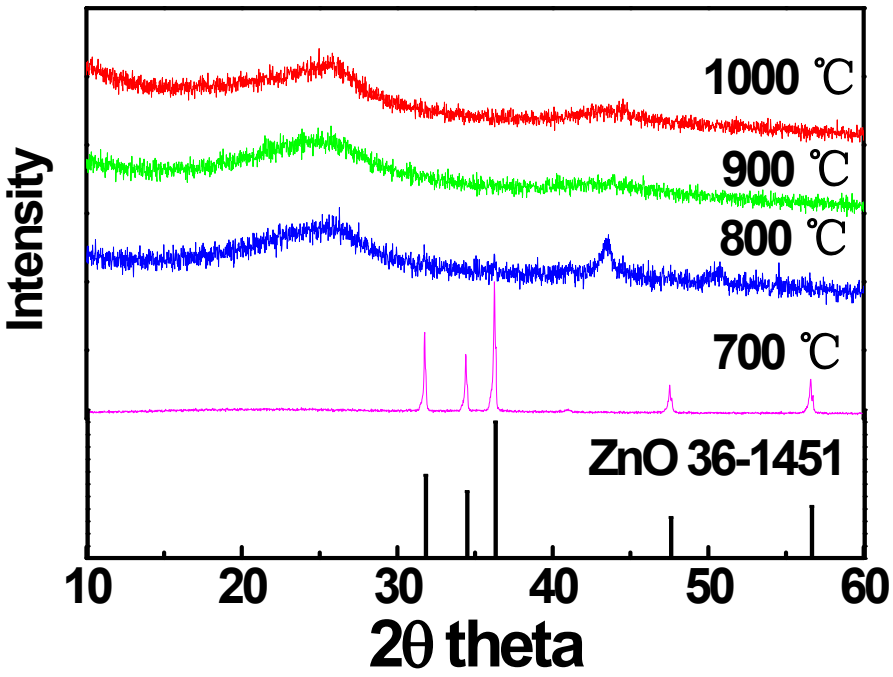

Fig S4. The XRD of as-prepared samples by pyrolysis at different temperatures.

The XRD spectra were used to characterize the presursors pyrolyzed at different temperatures. As shown in Fig S4, the samples at 700°C retained the residual ZnO precursor. When the temperature was raised to 800 °C, crystallized Fe_3C phase prevailed. However, no peaks characteristic of crystallize inorganic particles were observed after the temperature was raised above 900 °C, indicating the atomic dispersal of metal atoms within the carbon structures.

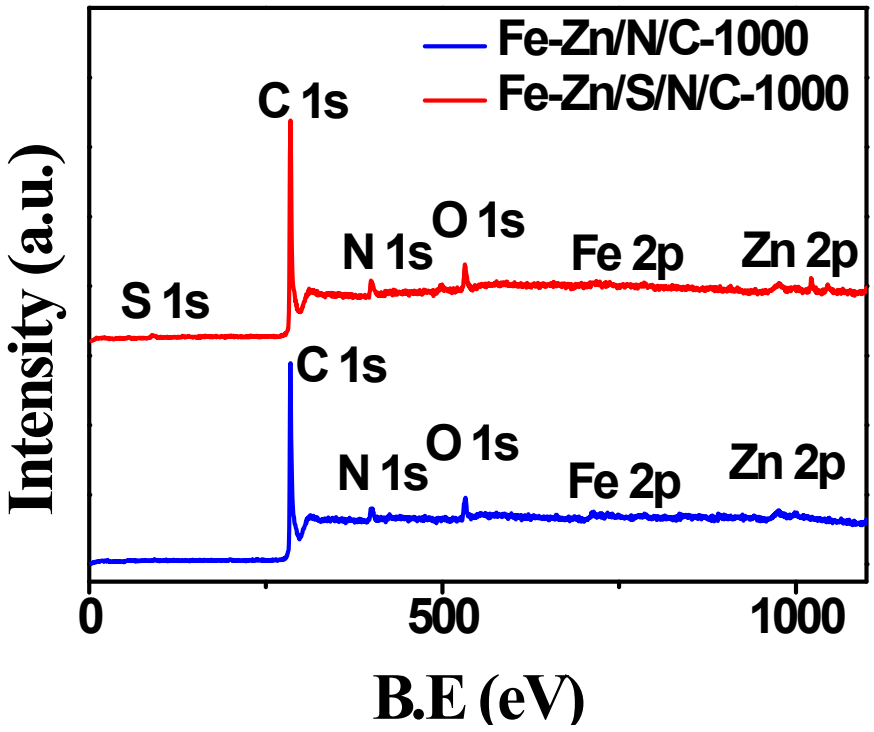

Fig S5. Wide range XPS spectra of the catalysts.

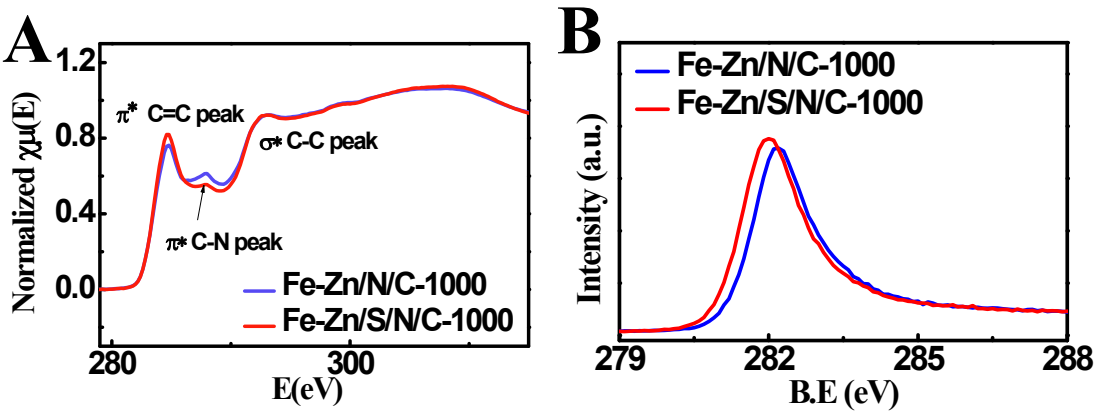

Fig S6. A) C K-edge NEXAFS spectra of the catalyst. B) C 1s XPS spectra.

Carbon K-edge near-edge X-ray absorption fine structure spectroscopy (NEXAFS) and X-ray photoelectron spectroscopy (XPS) were performed on Fe-Zn/N/C-1000 and Fe-Zn/S/N/C-1000 to provide complementary electronic information for the as-prepared catalyst (Fig S6 and Table S1), assigned to the transition to σ*C-O-C.[2] In addition the increase in I_{π^*}/I_{σ^*} from 0.83 to 0.89 after sulfur doping suggests that the content of graphitization structure was increased by sulfur doping, in agreement with the negative shift of the C 1s peak in XPS (Fig S4B).

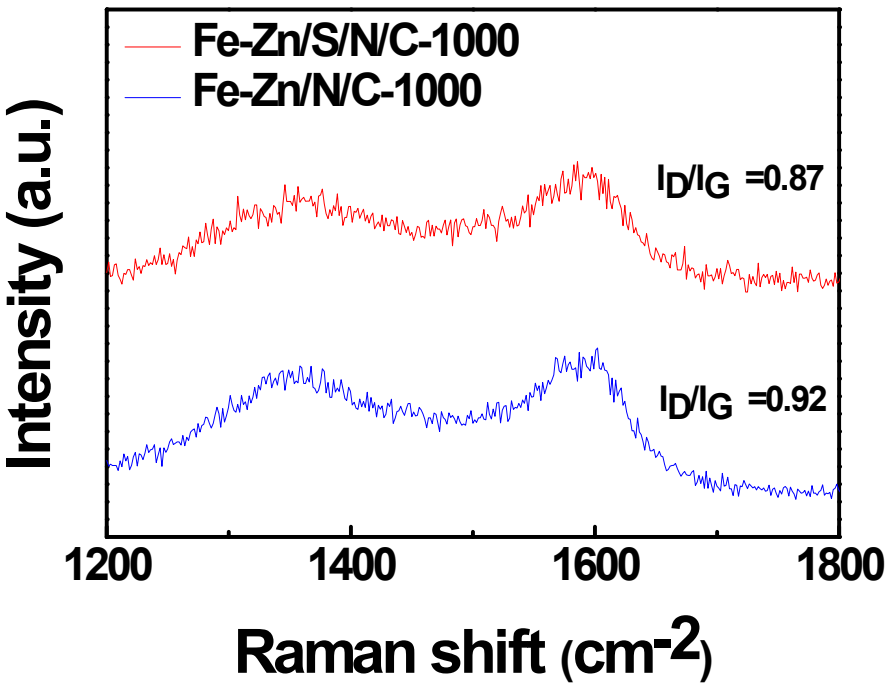

Fig S7. Raman spectra of Fe-Zn/N/C-1000 and Fe-Zn/S/N/C-1000.

The change caused by sulfur doping was also studied by Raman spectroscopy (Fig S7), in which two distinct bands at ~1345 cm^{-1} and 1590 cm^{-1} can be assigned to the defective/disordered sp^3 hybridized carbon (D band) and the crystallized graphitic sp^2 carbon (G band), respectively. The decrease of the I_D/I_G relative ratios from 0.92 to 0.87 also confirms improved graphitic nature after sulfur doping.

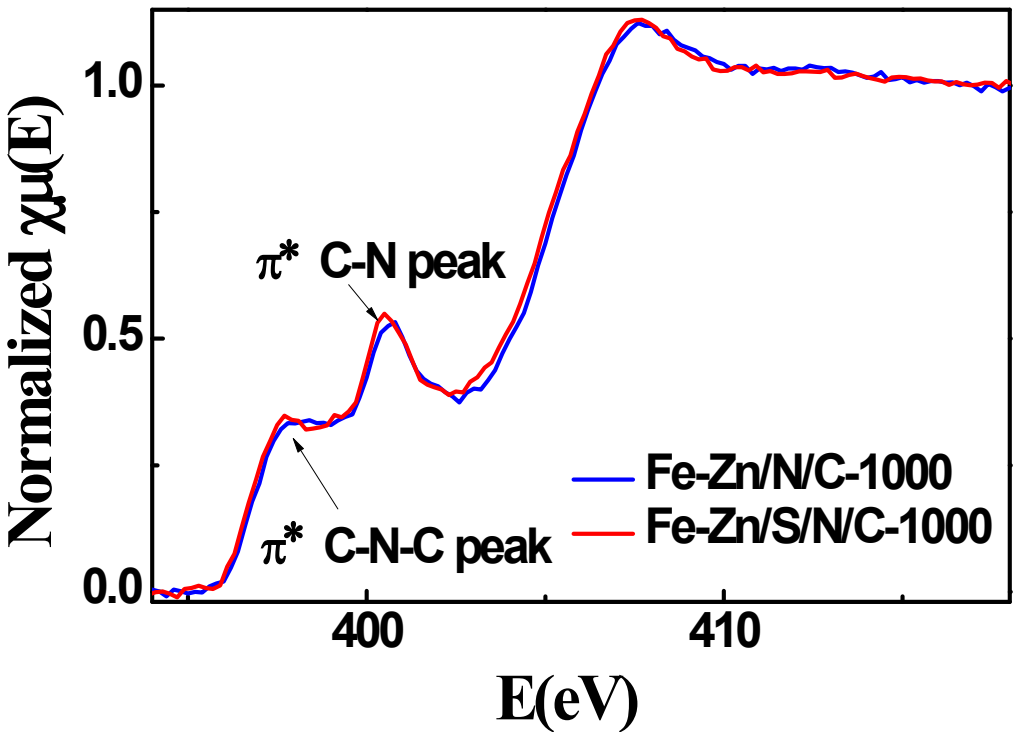

Fig S8. N K-edge XANES spectra of the catalysts.

Fig S8 displays N K-edge NEXAFS spectra for Fe-Zn/N/C-1000 and Fe-Zn/S/N/C-1000. The peak at ~398 eV assigned to pyridinic N indicate the presence of quaternary N with n-type doping. The peak at ~401 eV can be assigned to π* transitions and the peak at ~408 eV is due to C-N σ* transitions.[3]

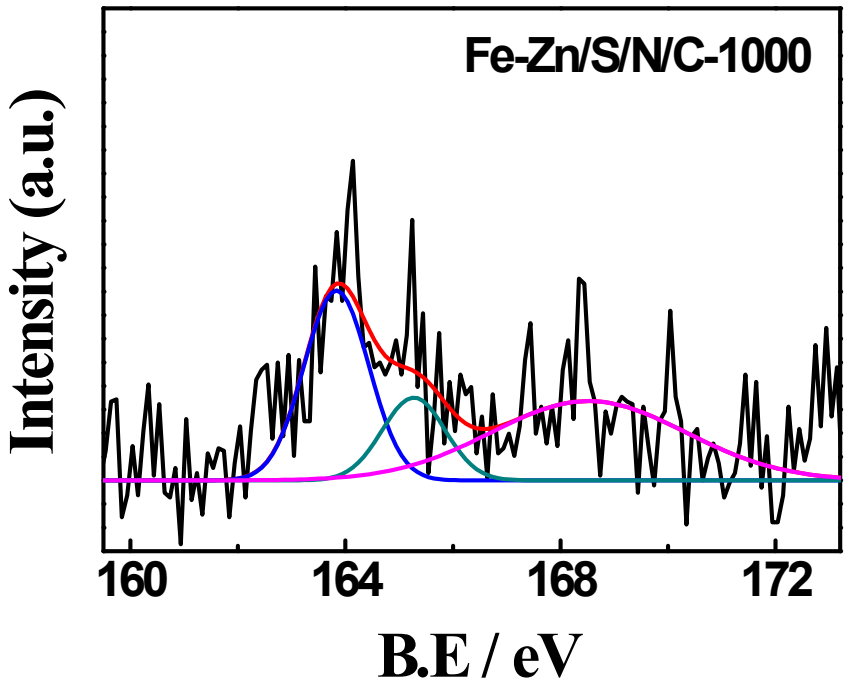

Fig S9. S 2p XPS spectrum of the Fe-Zn/S/N/C-1000.

Fig S9 shows the high-resolution spectrum of S 2p in Fe-Zn/S/N/C-1000. Two main peaks located at 163.8 and 165.2 eV are ascribed to the S $2p^{3/2}$ and S $2p^{1/2}$ peaks of sulfide species (C-S-C) in the sample. The peak at 168.5 eV is attributed to -C-SO*x*-C-,[4] suggesting that sulfur is bonded to carbon, in agreement with elemental mapping.

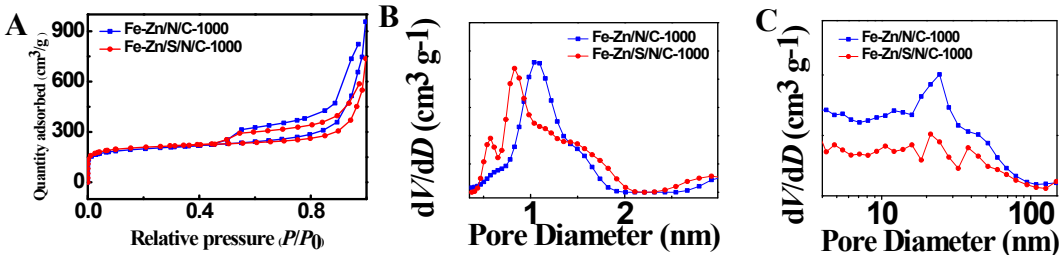

Fig S10. A) N_2 adsorption/desorption isotherms. B) micropore (NLDFT method). C) mesopore (BJH method) size distributions

The nitrogen sorption isotherms and pore size distributions (PSD) of Fe-Zn/N/C-1000 and Fe-Zn/S/N/C-1000 are shown in Fig S10 and summarized in Table S2. The Brunauer-Emmett-Teller (BET) surface area of as-prepared M-N-C catalysts increased from 741 $m^2 g^{-1}$ (Fe-Zn/N/C-1000) to 787 $m^2 g^{-1}$ (Fe-Zn/S/N/C-1000) after introducing sulfur doping in the carbon structures. Moreover, the micropore surface area of Fe-Zn/S/N/C-1000 is also larger than that of Fe-Zn/N/C-1000, increasing from 526 $m^2 g^{-1}$ to 639 $m^2 g^{-1}$. This is vital for ORR catalytic activity, since micropores within the carbon framework host active sites of M-N-C catalysts and facilitate ORR in acidic media. The mesopores in Fe-Zn/N/C-1000 and Fe-Zn/S/N/C-1000 are distributed mainly at 24 nm and 21 nm, respectively, according to the Barrett-Joyer-Halenda (BJH) model. The presence of mesopores and macropores is ascribed to residual ZnO acting as hard templates, which provide more space for evaporation of Zn at high temperature.

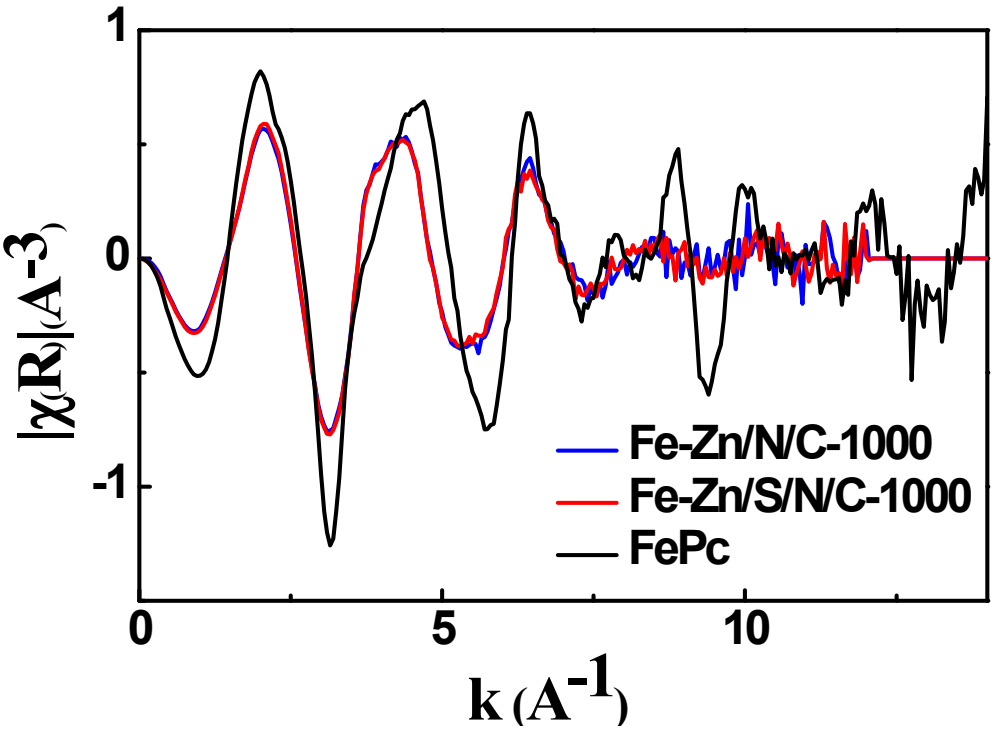

Fig S11. Fourier transforms of the Fe K-edge EXAFS oscillations of Fe-Zn/N/C-1000 and Fe-Zn/S/N/C-1000, reference samples FePc.

The k^2-weighted $\chi(k)$ signals of the Fe-Zn/N/C-1000, Fe-Zn/S/N/C-1000 and FePc show quite similar profiles (Fig S11), suggesting that the Fe atoms have similar coordination environments.

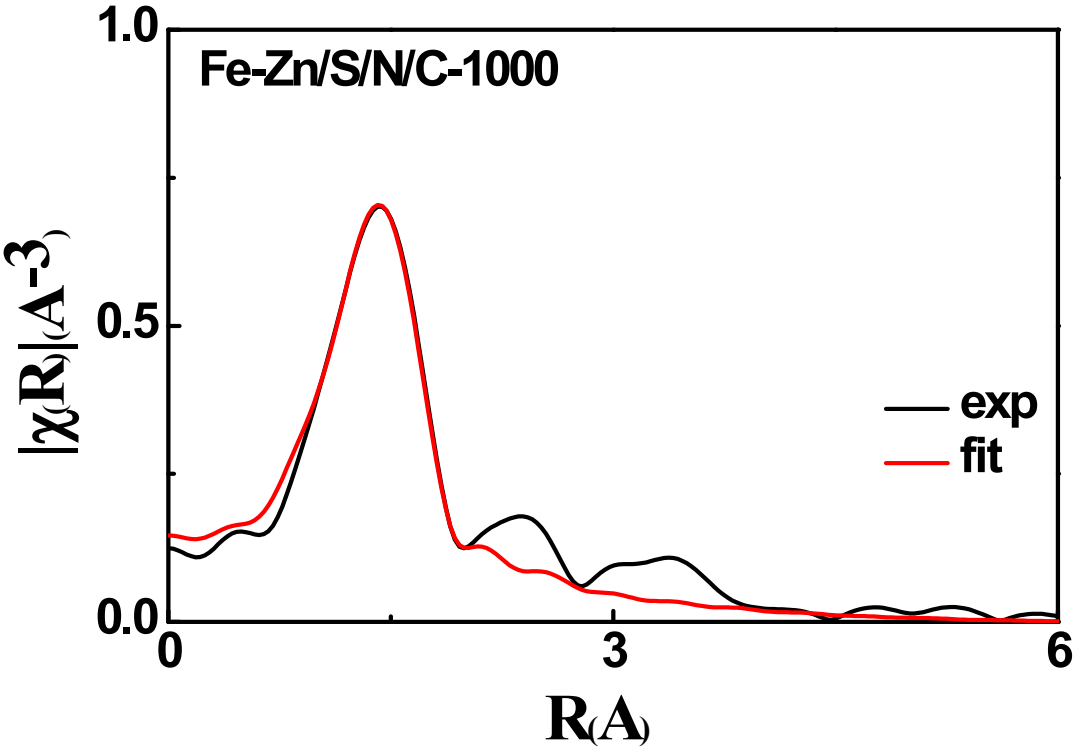

Fig S12. The corresponding EXAFS fitting curves for the samples.

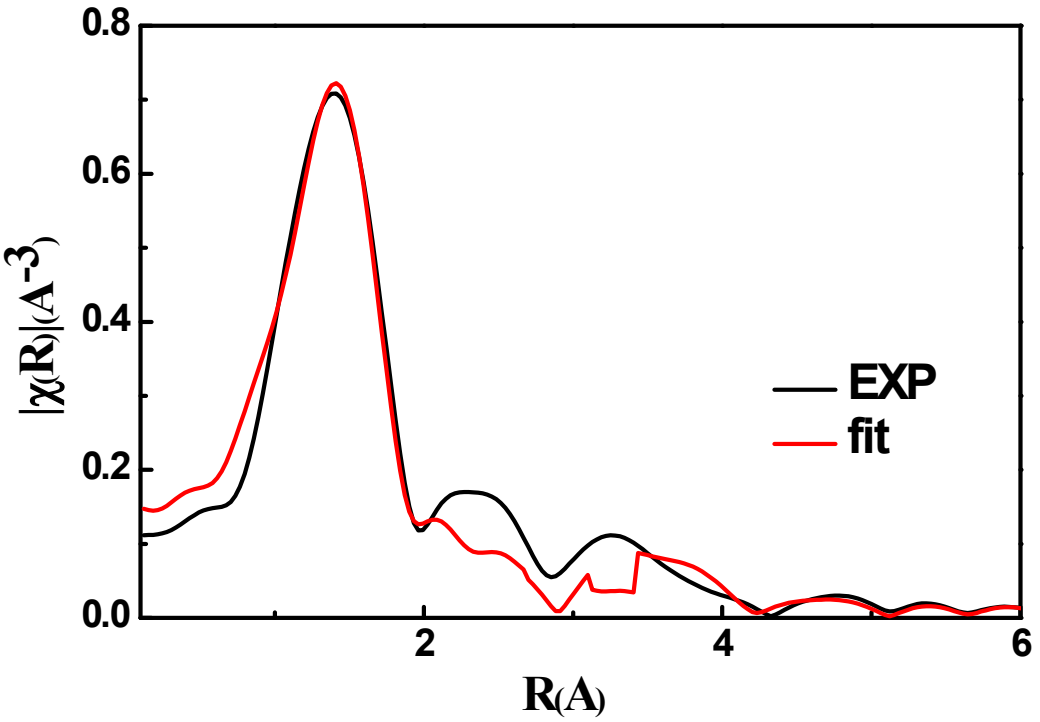

Fig S13. Magnitudes of Fourier-transforms of k^3-weighted (phase-uncorrected) EXAFS data for Fe-Zn/N/C-1000，and the fit in the Fourier transformed space for Fe-Zn/S/N/C-1000.

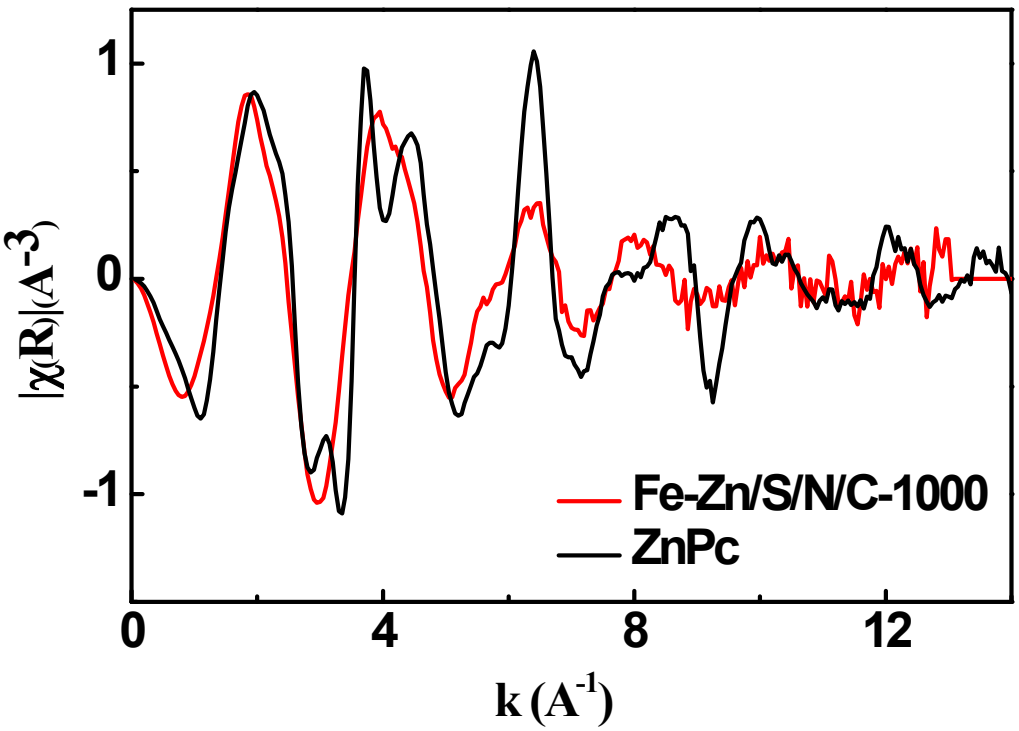

Fig S14. Fourier transforms of the Zn K-edge EXAFS oscillations of Fe-Zn/S/N/C-1000, reference samples ZnPc.

The k^2-weighted $\chi(k)$ signals of the Fe-Zn/S/N/C-1000 and ZnPc show quite similar profiles (Fig S14), suggesting similar coordination environments of the Zn atoms.

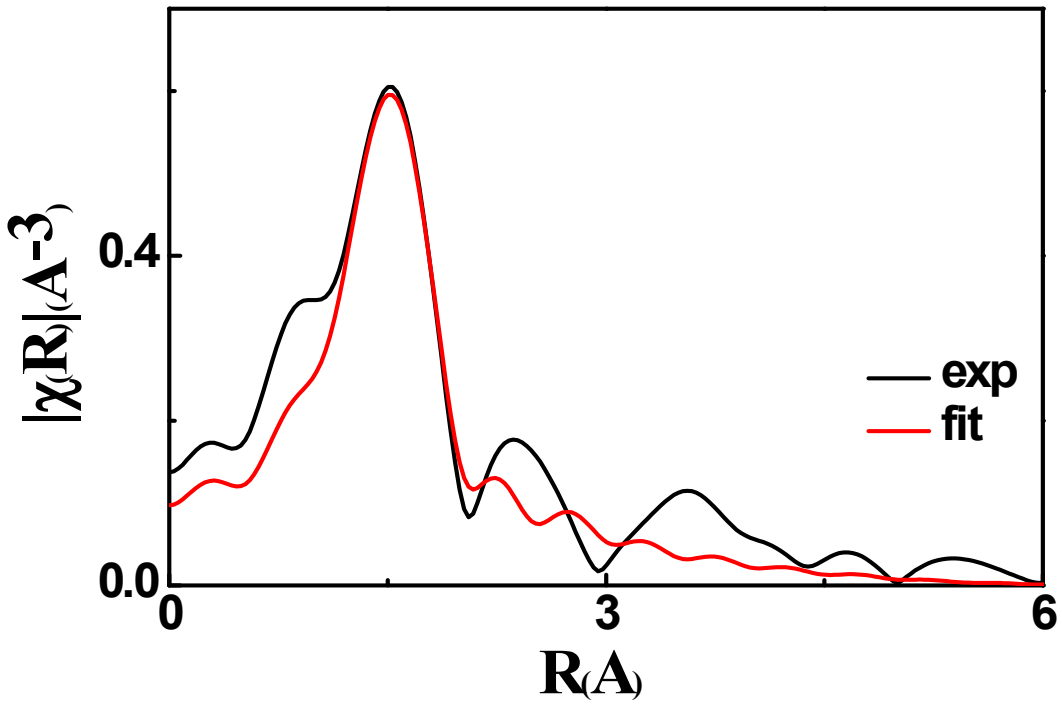

Fig S15. The fit in the Fourier transformed space for Fe-Zn/S/N/C-1000.

A

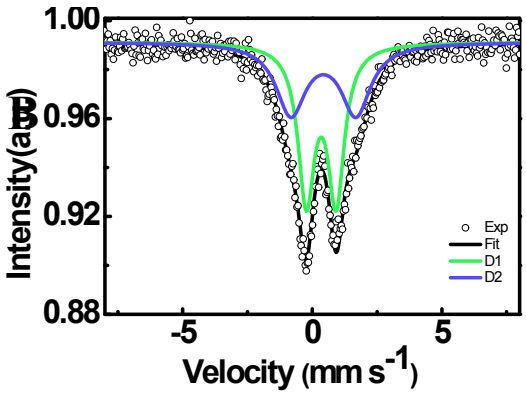

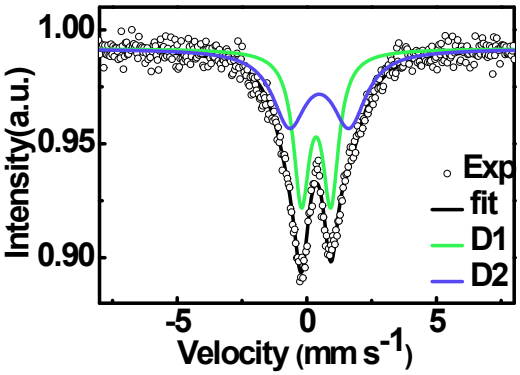

Fig S16. ^{57}Fe Mössbauer transmission characterization.

A-B.Experimental ^{57}Fe Mössbauer transmission spectra measured at 293 K for Fe-Zn/N/C-1000 (A) and Fe-Zn/S/N/C-1000 (B).

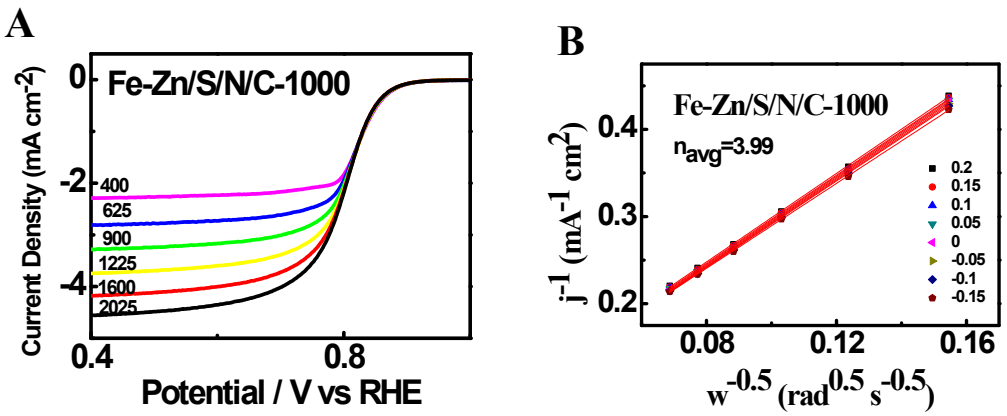

Fig S17. A) ORR polarization curves of Fe-Zn/S/N/C-1000 at different rotation speeds in 0.5 M H_2SO_4. B) K-L plots of different samples at various potentials.

The Fe-Zn/S/N/C-1000 sample delivers higher current densities at different rotation speeds, as shown in Fig S17. The K-L plot of the sample shows good linearity and a consistent slope, suggesting that first-order kinetics is correlated with the concentration of O_2 in the electrolyte during the ORR. The number of electrons transferred (n) is calculated to be 3.99, indicating that the catalyst can efficiently reduce oxygen in a direct four electron pathway.

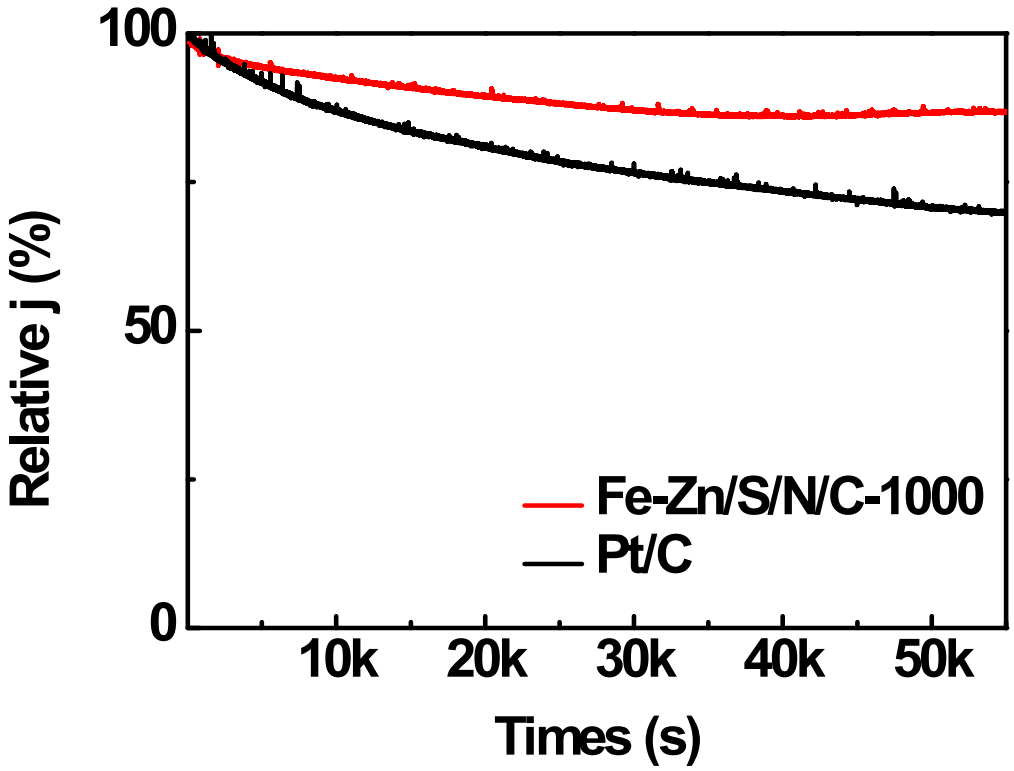

Fig S18. Current-time chronoamperometric responses of Fe-Zn/S/N/C-1000 and Pt/C at 0.533 V (at a rotation speed of 1600 rpm) over 55000s.

Fig S18 shows the current-time chronoamperometric responses of Fe-Zn/S/N/C-1000 and Pt/C at 0.533 V (RHE) in 0.5 M H_2SO_4, after more than 55000 s at a rotation speed of 1600 rpm. The Pt/C catalyst suffered 30.2 % loss of current density, while Fe-Zn/S/N/C-1000 catalyst lost only 13.3 %, demonstrating the excellent durability of Fe-Zn/S/N/C-1000 for ORR.

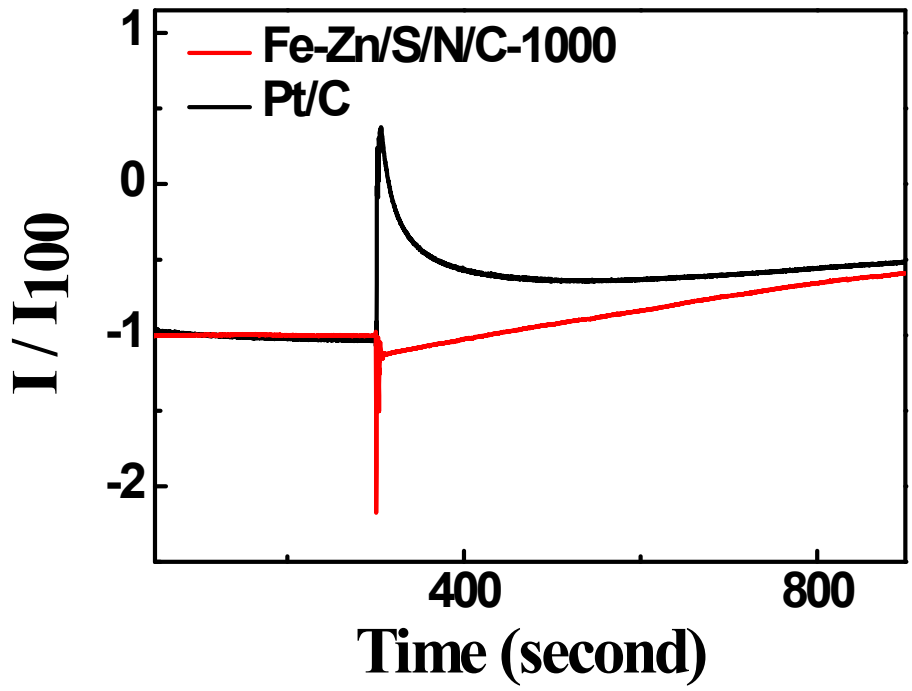

Fig S19. Cross-over tolerance test of the representative Fe-Zn/S/N/C-1000 samples before and after the addition of 10 vol% methanol into 0.5 M H_2SO_4.

Fig S19 shows the addition of methanol to a 0.5 M H_2SO_4 solution saturated with O_2, showed no noticeable change in ORR current at the Fe-Zn/S/N/C-1000, while the current for Pt/C decreased sharply. These results indicate that Fe-Zn/S/N/C-1000 has strong tolerance to crossover effects and is a promising catalyst for direct methanol fuel cells.[5-7]

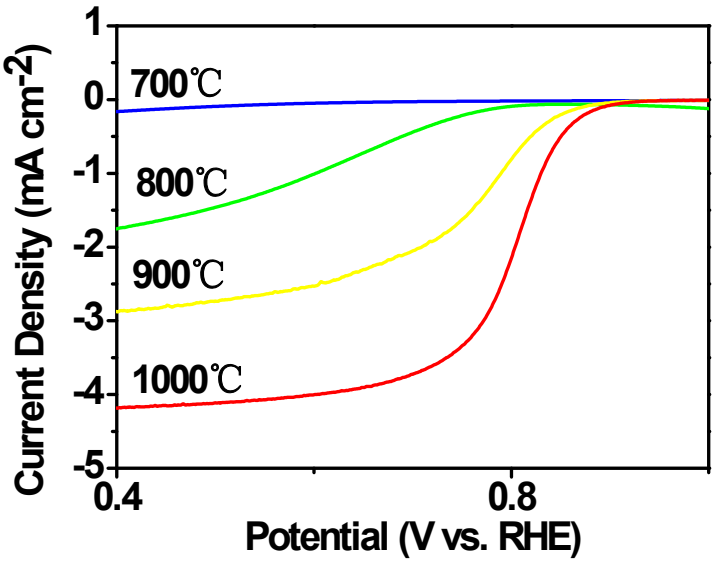

Fig S20. LSV curves of the catalysts pyrolyzed at different temperatures.

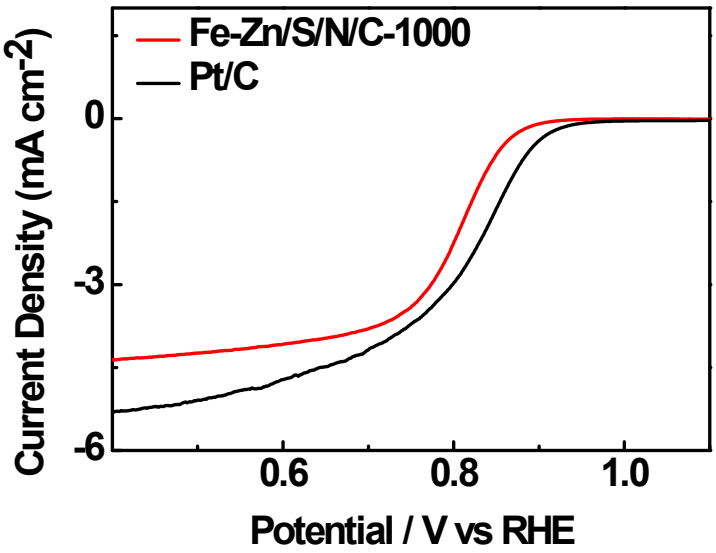

Fig S21. The ORR polarization curves of Fe-Zn/S/N/C-1000 and Pt/C, in O_2-saturated 0.1 M $HClO_4$ solution with a scan rate of 5 mV s^{-1} and a rotation rate of 1600 rpm at room temperature.

When compared to Fe-Zn/S/N/C-1000 and commercial Pt/C catalysts, the best ORR activity was achieved by Fe-Zn/S/N/C-1000, as judged by the half-wave ($E_{1/2}$) potentials in Figure S21. The $E_{1/2}$ of Fe-Zn/S/N/C-1000 was 0.809 V (RHE), which is 25 mV more negative than that of 20 wt.% Pt/C (0.834V), shows an excellent electroactivity on ORR.

Table S1. Summary of elemental compositions and TOF. C, N, O and S were detected by XPS, and Fe and Zn content were determined by ICP-OES

Sample	Element atomic ratio (%)						Fe (D1) wt %	TOF (0.8 V) $e\ site^{-1}\ s^{-1}$
	C	N	O	S	Fe	Zn		
Fe-Zn/N/C-1000	85.1	7.5	6.3	/	0.7	0.6	0.38	0.20
Fe-Zn/S/N/C-1000	84.9	7.3	6.2	0.4	1.2	1.7	0.58	0.64

Table S2. Texture properties of the catalysts.

Sample	S_{BET} ($m^2\ g^{-1}$)	S_{micro} ($m^2\ g^{-1}$)	S_{meso} ($m^2\ g^{-1}$)	V_{total} ($cm^3\ g^{-1}$)	V_{micro} ($cm^3\ g^{-1}$)	V_{meso} ($cm^3\ g^{-1}$)
Fe-Zn/N/C-1000	741	526	195	1.30	0.23	0.63
Fe-Zn/S/N/C-1000	787	639	133	0.97	0.27	0.36

Table S3. Best-fit parameters obtained from the analysis of the EXAFS spectra of Zn/Fe-DMSO-BM-1000 and FePc.

		CN	R(A)	σ^2 (A) * 10^{-3}	E_0 (eV)	R factor (%)
FePc	Fe-N	4	2.00	5.0	11.5	1.7
Fe-Zn/N/C-1000	Fe-O	1	1.87	6.0	2.8	0.5
	Fe-N	4	2.00	9.5	-3.9	
Fe-Zn/S/N/C-1000	Fe-O	1	1.87	4.0	4.5	0.1
	Fe-N	4	2.02	8.4	-2.9	
ZnPc	Zn-N	4	1.98	4.1	7.9	1.9
Fe-Zn/S/N/C-1000	Zn-N	4	2.00	8.1	4.4	0.7

CN is the coordination number, R is the interatomic distance, σ^2 is the Debye-Waller factor, E_0: the inner potential correction and R factor is the asymmetry parameter.

Table S4. Mössbauer parameters and relative absorption area obtained for each component from the fitting of the experimental spectrum recorded at room temperature. Isomer shift (IS), quadrupole splitting (QS), line width (LW) and relative spectral area % of each component. The isomer shift is given versus that of α-Fe.

	Fe-Zn/N/C-1000		Fe-Zn/S/N/C-1000	
Component	D1	D2	D1	D2
IS (mm s^{-1})	0.34	0.43	0.36	0.48
QS (mm s^{-1})	1.15	2.51	1.13	2.31
LW (mm s^{-1})	0.77	1.38	0.75	1.57
Area %	54.9	45.1	48.9	51.1
Assignment	$Fe(II)N_4$ LS	$Fe(II)N_4$ MS	$Fe(II)N_4$ LS	$Fe(II)N_4$ MS

Table S5. Summary of the ORR activity parameters at an electrode rotation speed of 1600 rpm.

Catalyst	Electrolytic Solution	Initial Potential (V vs. RHE)	Half-Wave Potential (V vs. RHE)
Fe-Zn/S/N/C-1000	0.5 M H_2SO_4	0.893	0.804
Fe-Zn/N/C-1000	0.5 M H_2SO_4	0.861	0.772
Zn/S/N/C-1000	0.5 M H_2SO_4	0.753	0.550
Fe-Zn/S/N/C-900	0.5 M H_2SO_4	0.872	0.775
Fe-Zn/S/N/C-800	0.5 M H_2SO_4	0.794	/
Fe-Zn/S/N/C-700	0.5 M H_2SO_4	/	/
Pt/C	0.5 M H_2SO_4	0.934	0.836

Notes and references

1. Y. J. Sa, D. J. Seo, J. Woo, J. T. Lim, J. Y. Cheon, S. Y. Yang, J. M. Lee, D. Kang, T. J. Shin, H. S. Shin, H. Y. Jeong, C. S. Kim, M. G. Kim, T. Y. Kim and S. H. Joo, *J Am Chem Soc*, 2016, **138**, 15046-15056.
2. H. B. Yang, J. Miao, S. F. Hung, J. Chen, H. B. Tao, X. Wang, L. Zhang, R. Chen, J. Gao, H. M. Chen, L. Dai and B. Liu, *Sci Adv*, 2016, **2**, e1501122.
3. H.-K. Kim, S.-M. Bak, S. W. Lee, M.-S. Kim, B. Park, S. C. Lee, Y. J. Choi, S. C. Jun, J. T. Han and K.-W. Nam, *Energy & Environmental Science*, 2016, **9**, 1270-1281.
4. P. Chen, T. Zhou, L. Xing, K. Xu, Y. Tong, H. Xie, L. Zhang, W. Yan, W. Chu, C. Wu and Y. Xie, *Angew Chem Int Ed Engl*, 2017, **56**, 610-614.
5. U. I. Kramm, J. Herranz, N. Larouche, T. M. Arruda, M. Lefevre, F. Jaouen, P. Bogdanoff, S. Fiechter, I. Abs-Wurmbach, S. Mukerjee and J. P. Dodelet, *Phys Chem Chem Phys*, 2012, **14**, 11673-11688.
6. U. I. Kramm, I. Herrmann-Geppert, J. Behrends, K. Lips, S. Fiechter and P. Bogdanoff, *J Am Chem Soc*, 2016, **138**, 635-640.
7. A. Zitolo, V. Goellner, V. Armel, M. T. Sougrati, T. Mineva, L. Stievano, E. Fonda and F. Jaouen, *Nat Mater*, 2015, **14**, 937-942.